Electronic Supplementary Information

High-throughput and directed microparticles manipulation in complex-shaped maze chambers based on travelling surface acoustic waves

Wanyu Weng†[a], Hemin Pan†[b], Yancheng Wang[a*]

[a.] *State Key Laboratory of Fluid Power and Mechatronic Systems, School of Mechanical Engineering, Zhejiang University, Hangzhou 310027, China.*

[b.] *Key Laboratory of Advanced Manufacturing Technology of Zhejiang Province, School of Mechanical Engineering, Zhejiang University, Hangzhou 310027, China*

† These authors contributed equally to this work.

**Corresponding author: Yancheng Wang*

E-mail: yanchwang@zju.edu.cn; Tel.: (+86) 571-87951906; Fax: (+86) 571-87951145

Supplementary Materials

The PDF file includes:

Fig. S1 to S9

Table S1 to S2

Legends for Movies S1 to S6

Other Supplementary Materials for this manuscript includes the following:

Movies S1 to S6

Supplementary Figures.

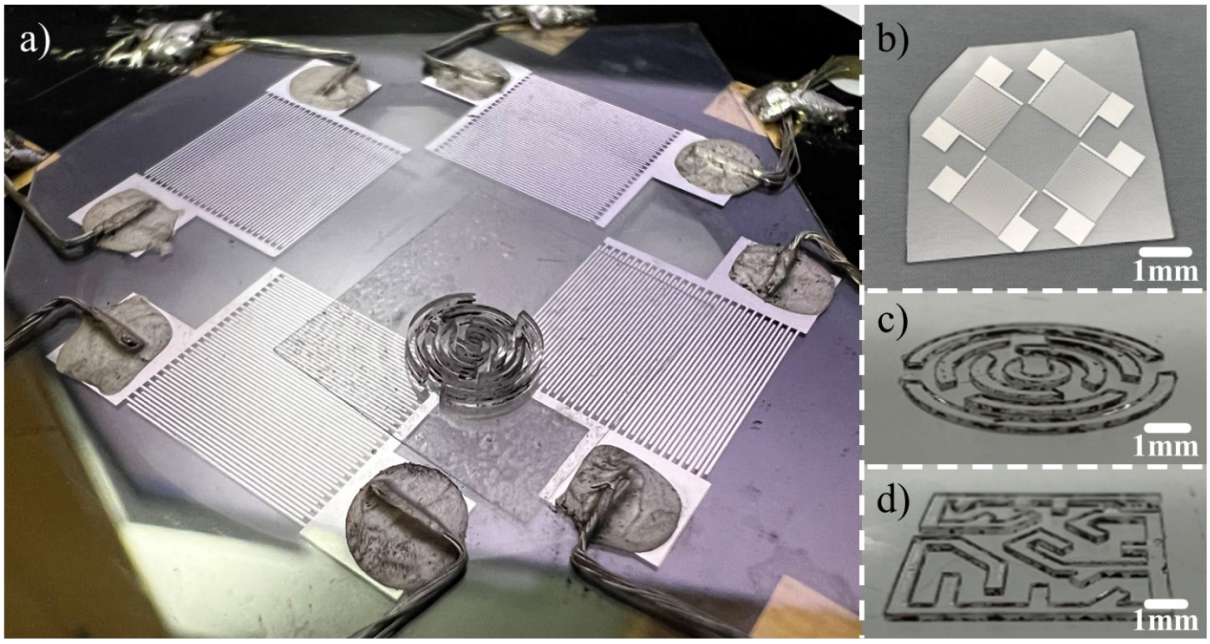

Fig. S1 The optical images of TSAW-based device. (a) Experimental setup during the tests. (b) The image of orthogonally arranged IDTs. (c) The image of round-shaped maze chamber. (d) The image of square-shaped maze chamber.

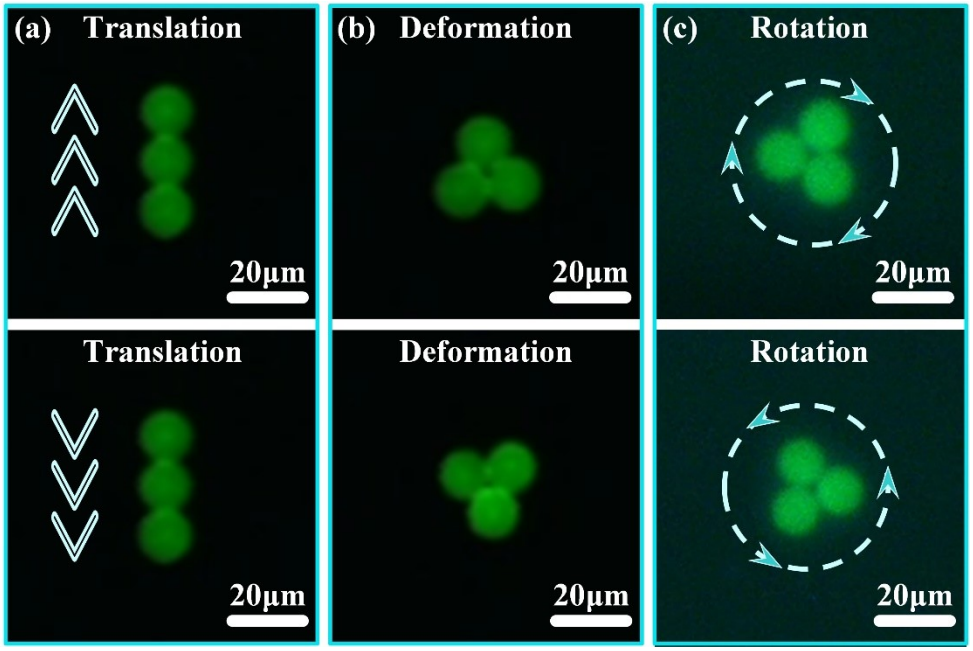

Fig. S2 Precise capture and manipulation of single PS trimer using IDTs array: (a) The directional translation of Linear trimer manipulated by modulating the relative phase of IDTs array. (b) The reconfigurable deformation of PS trimer by modulating the exciting frequencies of IDTs array. (c) The controllable rotation of PS trimer by modulating the input voltages of IDTs array.

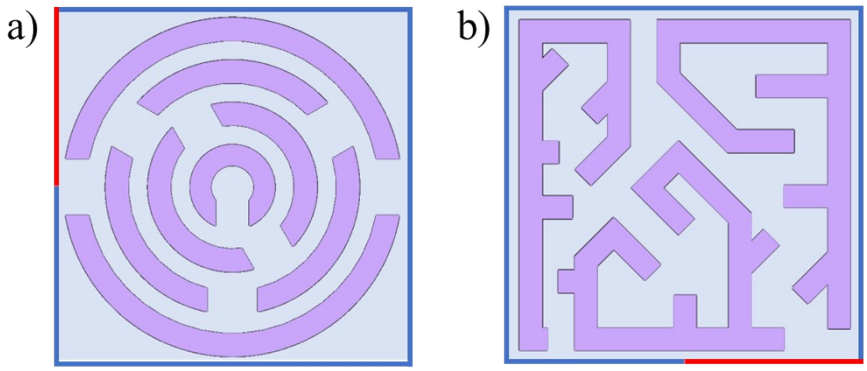

Fig. S3 FDM model of the total acoustic pressure field distribution. (a) The round-shaped maze model. (b) The square-shaped maze model. The red boundaries are the normal acceleration boundaries; the blue boundaries are the plane wave radiation boundaries.

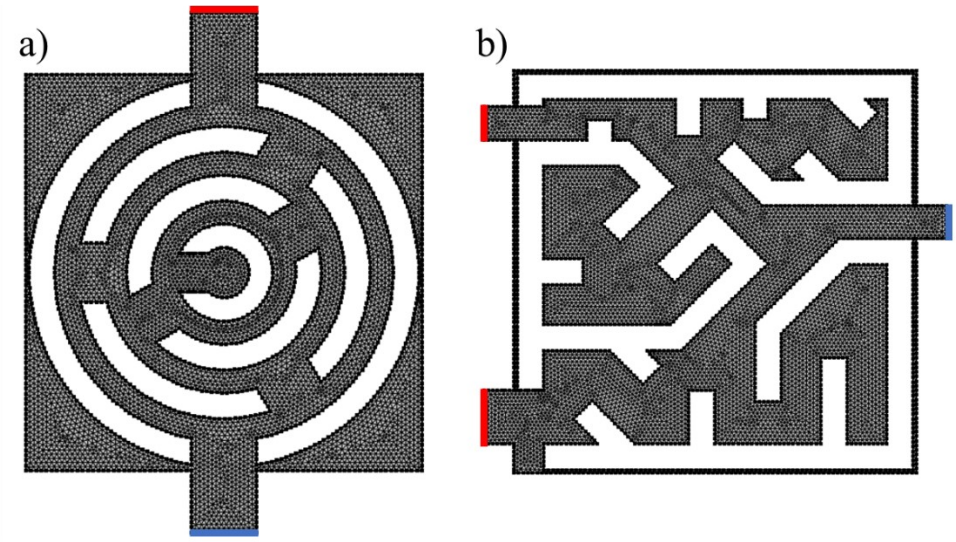

Fig. S4 FDM model of the acoustic streaming velocity distribution. (a) The round-shaped maze model. (b) The square-shaped maze model. The red boundaries are the particle release boundaries; the blue boundaries are the particle leaving boundaries.

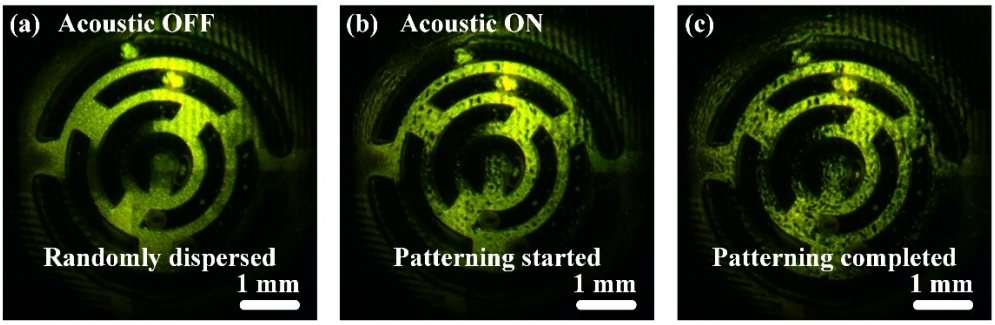

Fig. S5 The 10 μm PS microparticle manipulation pattern within the round-shape maze chamber. (a) The randomly dispersed microparticles with acoustics off. (b) The microparticles started to pattern with the excitation combination of IDTs (K_{I} and $K_{\mathrm{I}}^{'}$). (c) The patterning of microparticles within the round-shaped maze chamber was completed.

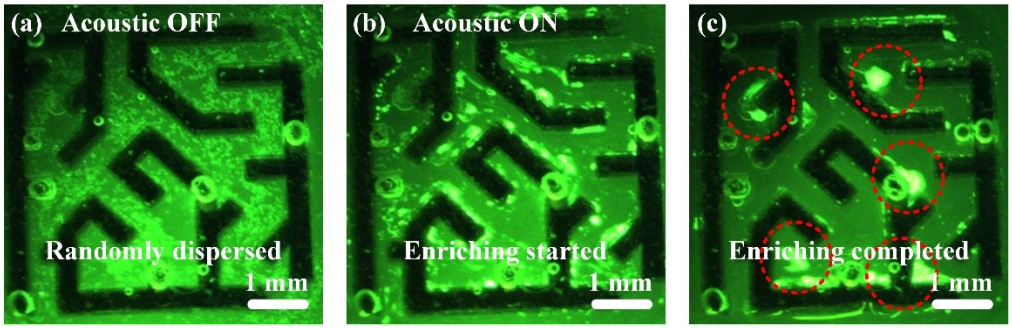

Fig. S6 The enrichment of the suspended microparticle waste inside the square-shaped maze chamber. (a) The randomly dispersed microparticles with acoustics off. (b) The microparticles started to enrich at the sharp structures of the chamber wall with all IDTs activated. (c) The concentration and recycling of microparticles waste within the square-shaped maze chamber was completed.. (a) The randomly dispersed microparticles with acoustics off. (b) The microparticles started to enrich at the sharp structures of the chamber wall with all IDTs activated. (c) The concentration and recycling of microparticle waste within the square-shaped maze chamber were completed.

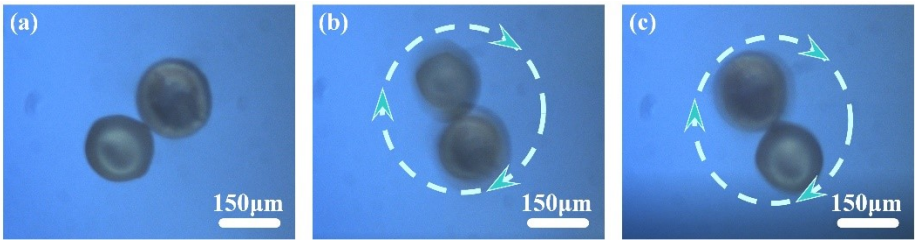

Fig. S7 The manipulation of brine shrimp egg dimer by acoustic streaming effects within annular chamber. (a) Shrimp egg dimers remain stationary with acoustics off. (b) The shrimp egg dimer started to rotate clockwise with single IDT activated. (c) The shrimp egg dimer rotated clockwise by 180° with single IDT activated.

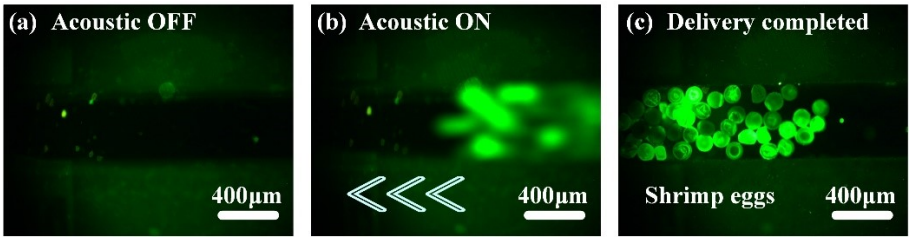

Fig. S8 The directional transportation of brine shrimp eggs by acoustic streaming effects within straight flow channel. (a) No shrimp eggs in the outlet flow channel with acoustics off. (b) The numerous shrimp eggs started to move towards the outlet flow channel with single IDT activated. (c) The shrimp eggs reach the outlet of the flow channel driven by the acoustic streaming.

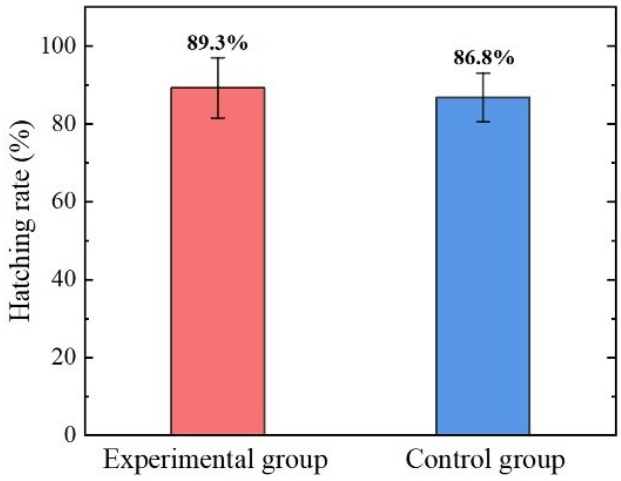

Fig. S9 The hatching rates of brine shrimp eggs in the controlled experiment. The shrimp eggs from the experimental group were incubated after undergoing acoustic streaming manipulation, while the shrimp eggs from the control group were incubated without any treatment before.

Table S1 The detailed parameters for the calculation

Parameter	Symbol	Value
Dynamic viscosity of the water	η	1.01×10^{-3} Pa·s
Radius of microparticle	R	$5\sim10\times10^{-6}$ m
Geometry-dependent factor of chamber	Ψ	0.35
Amplitude of acoustic pressure	p_a	$0\sim8\times10^{5}$ Pa
Density of the microparticle	ρ_p	1080 kg/m^3
Density of the liquid	ρ_l	1000 kg/m^3
Frequency of the TSAW beams	f	8.8-10.0 MHz
Acoustic velocity in the liquid	c_l	1500 m/s
Moving velocity of microparticle	v_p	0~154.7 μm/s

Table S2 The force characterization for microparticle

Force	Magnitude(N)
Acoustic radiation force	$0\sim1.117\times10^{-15}$
Viscous force	$0\sim1.564\times10^{-12}$
Buoyancy	5.237×10^{-13}
Gravity	5.656×10^{-13}

Supplementary Movies.

Movie S1. Microparticles moving trends in the round-shaped maze chamber.

Movie S2. Microparticles moving trends in the square-shaped maze chamber.

Movie S3. Precise capture and manipulation of single PS trimer using IDTs array.

Movie S4. The microparticle manipulation pattern within the round-shape maze chamber.

Movie S5. The enrichment of the suspended microparticle waste inside the square-shaped maze chamber.

Movie S6. The manipulation of brine shrimp eggs by acoustic streaming effects.